Heliyon 10 (2024) e31766

Contents lists available at ScienceDirect

Heliyon

journal homepage: www.cell.com/heliyon

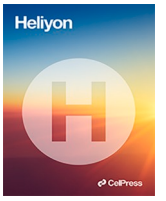

Research article

Towards greener futures: SVR-based CO_2 prediction model boosted by SCMSSA algorithm

Oluwatayomi Rereloluwa Adegboye [a], Afi Kekeli Feda [b], Ephraim Bonah Agyekum [c], Wulfran Fendzi Mbasso [d,*], Salah Kamel [e]

[a] Engineering Management Department, University of Mediterranean Karpasia, Mersin-10, Turkey
[b] Advanced Research Centre, European University of Lefke, Mersin-10, Turkey
[c] Department of Nuclear and Renewable Energy, Ural Federal University Named After the First President of Russia Boris Yeltsin, 19 Mira Street, Ekaterinburg, 620002, Russia
[d] Laboratory of Technology and Applied Sciences, University Institute of Technology, University of Douala, PO Box: 8698 Douala, Cameroon
[e] Department of Electrical Engineering, Faculty of Engineering, Aswan University, Aswan, 81542, Egypt

ARTICLE INFO

Keywords:
Sine cosine perturbation
Chaotic perturbation
Mirror imaging strategy
Salp swarm algorithm (SCMSSA)
Support vector regression (SVR)

ABSTRACT

This research presents the utilization of an enhanced Sine cosine perturbation with Chaotic perturbation and Mirror imaging strategy-based Salp Swarm Algorithm (SCMSSA), which incorporates three improvement mechanisms, to enhance the convergence accuracy and speed of the optimization algorithm. The study assesses the SCMSSA algorithm's performance against other optimization algorithms using six test functions to show the efficacy of the enhancement strategies. Furthermore, its efficacy in improving Support Vector Regression (SVR) models for CO_2 prediction is assessed. The results reveal that the SVR-SCMSSA hybrid model surpasses other hybrid models and standard SVR in terms of training and prediction accuracy by obtaining 95 % accuracy. Its swift convergence, precision, and resistance to local optima position make it an excellent choice for addressing complex problems such as CO_2 prediction, with critical implications for sustainability efforts. Moreover, feature importance analysis by SVR-SCMSSA offers valuable insights into the key contributors to CO_2 prediction in the dataset, emphasizing the significance and impact of factors such as fossil fuel, Biomass, and Wood as major contributors to CO_2 emission. The research suggests the adoption of the SVR-SCMSSA hybrid model for more accurate and reliable CO_2 prediction to researchers and policymakers, which is essential for environmental sustainability and climate change mitigation.

1. Introduction

Climate change is viewed today as the greatest threat to humanity's survival [1,2]. Despite the 2015 International Paris Agreement aimed at reducing greenhouse gas emissions, global temperatures have risen primarily due to the increased global reliance on fossil fuels. Eighty percent of the world's energy consumption is derived from the use of fossil fuels, a practice that plays a pivotal role in the rapid expansion of globalization and industrialization [3,4]. It's a well-established fact that the emissions of greenhouse gases, most

* Corresponding author.
E-mail addresses: aoluwatayomi@gmail.com (O.R. Adegboye), kekelifeda@gmail.com (A.K. Feda), agyekumephraim@yahoo.com (E.B. Agyekum), fendzi.wulfran@yahoo.fr (W.F. Mbasso), skamel@aswu.edu.eg (S. Kamel).

https://doi.org/10.1016/j.heliyon.2024.e31766
Received 22 November 2023; Received in revised form 18 May 2024; Accepted 21 May 2024
Available online 22 May 2024

notably carbon dioxide, have detrimental effects on the environment, particularly with regard to global warming [5,6]. These emissions are mostly caused by burning fossil fuels to produce electricity and heat.

According to the scientific community, carbon dioxide releases are the primary cause of global warming [7]. For the purpose of establishing effective energy policies and preparing for climate change, it is crucial to predict CO_2 emissions from the perspective of energy use [7]. Anticipating CO_2 emissions may be helpful in estimating future increases in global temperatures and even in assessing the possible costs of reducing emissions and the possible advantages of protecting against such increases. Furthermore, according to the Copenhagen Accord, increases in global temperatures have to be limited to less than 2 °C. This means that by 2050, global emissions must drop by 50–80 % from 1990 levels [8–11]. As 2050 draws near, a number of methods for capturing carbon are already proposed to reduce the release of carbon dioxide and minimize global warming to 2 °C [12–14]. CO_2 emissions prediction, in combination with carbon capture technology, can help investigate the extent to which the continuous reinforcement of international climate policy can result in a significant drop in CO_2 emissions to meet the 2 °C target [15]. Otherwise, the governments must implement more stringent climate regulations. Over the past few years, there have been significant advancements in artificial intelligence (AI) technology, particularly in its application to forecasting [16,17]. AI stands out due to its ability to self-learn and handle intricate non-linear issues, allowing it to consider all the relevant parameters in forecasting, resulting in improved predictive outcomes [18,19]. Ahmed et al. focused on improving the accuracy of streamflow forecasting, a critical aspect of water planning and decision-making [20]. They combined a Multi-layer Perceptron (MLP) model with the Nuclear Reaction Optimization (NRO). The researchers used a streamflow record gathered from the High Aswan Dam (HAD) station over 13 decades to assess the hybrid model's effectiveness. The novel method was contrasted against nine different hybrid MLP-based algorithms, as well as the conventional neural networks. According to the research's findings, adding MLP to the NRO algorithm provides an accurate and dependable method for monthly streamflow prediction that offers quick convergence and a high degree of stability. Abedinia et al. proposed an innovative forecasting approach that combines a neural network with an Enhanced Smell Shark Optimization algorithm, significantly improving the learning capabilities of the forecasting engine in collecting intricate signal mappings [21]. Additionally, this combination prevents the forecasting engine from becoming trapped in local minimums. The neural network's parameters are adjusted using the metaheuristic technique. This forecasting approach was carefully applied to an engineering real-life scenario to validate its effectiveness. The resulting findings clearly demonstrate this approach's superior efficacy when compared to alternative prediction techniques. Masood et al. presented the ELM-SO, which combines the Snake Optimization Algorithm and the Extreme Learning Machine (ELM) [22]. Meteorological parameters and air quality inputs were used to assess this model. With a root mean square error of 30.325 $\mu g/m^3$ and a squared correlation coefficient of 0.928, the results show that ELM-SO performs better than other compared techniques in terms of prediction. Lashgari et al. [23] presented a novel strategy to improve Taiwan's transportation energy consumption predictions. The research introduced an Improved variant of the Emperor Penguin Optimizer (IEPO). The IEPO algorithm, which takes into account variables such as population, GDP growth rate, and total yearly vehicle kilometers, was utilized to maximize the parameters of three separate models quadratic, exponential, and linear used in the forecasting process. As a useful tool for decision-making, the simulation results demonstrated the excellent efficiency of the IEPO-based transportation energy consumption forecasts across all models used. Ismael et al. introduced a hybrid model, which integrates a Spotted Hyena Optimizer (SHO) with support vector machine (SVR) techniques, to forecast the flux pressure in Vacuum Membrane Distillation (VMD) [24]. This hybrid model, validated against experimental data, was compared with various machine learning tools such as artificial neural networks (ANNs), classical SVR, and multiple linear regression (MLR). Notably, the results demonstrate the superior accuracy of the SVR-SHO model, achieving a correlation coefficient (R) of 0.94 in flux pressure prediction. Quin et al. introduced a new Marine Predator Algorithm (MPA) that addresses the drawbacks of poor convergence accuracy and the propensity for standard MPA to enter a local optimum state by combining it with the Golden sine algorithm with Elite opposition-based learning (EGMPA) [25]. Additionally, the authors introduced a novel multi-kernel support vector regression that solves the selection of variables problem by using multiple kernel functions. The study inputs are China's carbon dioxide emission statistics from 1965 to 2020. China's carbon dioxide emissions are predicted using the suggested method over the span of the "14th Five-Year Plan". The outcomes proved that the suggested method improves China's CO_2 emissions forecasting precision. Jalaee et al. suggested a novel Artificial Neural Network combined with a Cuckoo Optimization Algorithm called COANN [26]. The Correlation Coefficient (CC), Mean Absolute Error (MAE), Root Mean Square Error (RMSE), and Mean Squared Error (MSE) between the model's result and the real dataset are used to assess the performance of the COANN. Finally, a COANN forecast of global CO_2 emissions by 2050 is presented. The results demonstrated that COANN is an effective and trustworthy technique for tracking global warming. An Artificial Neural Network (ANN) model trained using the Grey Wolf Optimizer (GWO) technique was presented by Uzlu to forecast Turkey's GHG emissions [27]. Statistics on energy consumption, the Gross domestic product (GDP), population, pace of urbanization, and generation of renewable energy were utilized as forecast factors. The outputs of the novel ANN-GWO model were contrasted using numerous error criteria to the performance of the ANN-ABC (Artificial Bee Colony), the ANN-BP (Back-Propagation), and ANN-TLBO (Teaching–Learning–Based Optimization) models in order to assess the precision of the suggested approach. Based on the average relative error values computed during the test, ANN-GWO outperforms ANN-ABC by 35.29 %, ANN-BP by 32.23 %, and ANN-TLBO by 19.33 %. Three situations were used to estimate GHG emissions through 2030 using the ANN-GWO. The results showed that GHG emissions are anticipated to exceed government projections and that the GWO optimization algorithm is useful for projecting GHG emissions.

The No-Free-Lunch (NFL) theorem highlights a fundamental principle: there's no universal optimizer that excels in solving every optimization problem and surpasses all other methods [28–30]. Instead, the performance of an optimizer may vary, excelling in some cases while falling short in others. Even though the aforementioned algorithm exhibits outstanding performance, there is a tendency to fall short in complex optimization problems, according to NFL. This opens up numerous opportunities, including the development of entirely new optimization algorithms or the refinement of existing ones, which may have the potential to surpass their predecessors in

the context of CO_2 emissions prediction. Secondly, AI models and machine learning techniques require fine-tuning their hyper-parameters to improve their prediction accuracy in CO_2 emission prediction. These research gaps form the impetus of this research endeavour to enhance the traditional Salp Swarm Algorithm (SSA) as a parameter adjustment mechanism for the CO_2 prediction model. The Salp Swarm Algorithm (SSA), one of the most current swarm optimization techniques, was introduced by Mirjalili et al. [31]. The fundamental principle of the SSA algorithm is to use the salps chain notion to simulate the swarming activity of salps in the water. The SSA algorithm was selected for its advantages, including efficiency, adaptability, simplicity in implementation, and a small number of initialization parameters. The SSA, however, has limitations in terms of population diversity and local optima [32,33]. To address these issues, an improved version of SSAcalled Sine cosine perturbation with Chaotic perturbation and Mirror imaging strategy-based Salp Swarm Algorithm (SCMSSA) is introduced in this study to improve the Support Vector Regression model prediction accuracy. The SVR-SCMSSA builds on SCMSSA's improved exploration and exploitation ability to find the most optimal parameters to a given optimization problem, through the three newly introduced enhancement techniques, namely Sine Cosine Strategy, Mirror Imaging Technique, and Chaotic Perturbation, preventing the local optima's trap and enhancing solution diversity.

The subsequent sections of this paper are structured as follows: section 2 provides essential background information about the original Salp Swarm algorithm, section 3 outlines the specifics of the newly proposed SCMSSA algorithm, and Section 4 elaborates on the steps involved in building the SVR-SCMSSA CO_2 prediction model, Section details 5 the data description and preprocessing, in Section 6 the conducted experiments on CO_2 prediction and the corresponding results are discussed. Finally, Section 7 presents the concluding remarks of this study.

2. Original Salp Swarm Algorithm (SSA)

Mirjalili et al. introduced the Salp Swarm Algorithm (SSA), as a recent addition to the group of swarm optimization algorithms [31]. The goal behind SSA is to mimic the collective habit of salps. Throughout their aquatic existence, salps engage in a distinctive swarming habit referred to as the "salp chain" that is also employed in their quest for food. The SSA population consists of two distinct groups: leaders and followers. The leader, situated at the forefront of the salps chain, plays a pivotal role in deciding where to move to, where to feed, and periodically refreshing these target site options. The rest of the individuals are referred to as "followers" since they all follow the leader in succession, forming a chain pattern. Every single point in the n dimensions search area represents a possible solution with n representing the number of variables pertinent to the problem at hand. Additionally, the concept of "food supply," symbolized by F stands for the objective that the salps are seeking. This scenario is depicted by Equation (1).

$$x_j^1 = \begin{cases} F_j + r_1\left(\left(ub_j - lb_j\right)r_2 + lb_j\right) & r_3 \geq 0.5 \\ F_j - r_1\left(\left(ub_j - lb_j\right)r_2 + lb_j\right) & r_3 < 0.5 \end{cases} \tag{1}$$

x_j^1 and F represent respectively the leader and the target's position in the jth dimension, while ub_j and lb_j are the upper and lower boundaries of the Salps position components. $r2$ and $r3$ scalar values were randomly selected from the [0,1] interval. The critical control parameter is $r1$, responsible for stabilizing the exploration and exploitation. $r1$ is expressed in Eq (2):

$$r1 = 2e^{-\left(\frac{4t}{T}\right)^2} \tag{2}$$

Here, the present number of iterations and the highest number of potential iterations are denoted by t and T, respectively. The equation given in equation (3) is used for updating the followers' positions such that i > 2.

$$x_j^i = \frac{1}{2}\left(x_j^i + x_j^{i-1}\right) \tag{3}$$

Table 1
Algorithm 1: Pseudocode SSA.

```
Initialize the population randomly.
Obtain the fitness of all salps
Set FoodPosition as the leader salp and fitness of leader as FoodFitness
While (end condition not met) do
Update r1 by Eq. (2)
For (every salp (x_j)) do
If ((i = < N/2) then
Update the position of leader by Eq. (1)
Else
Update the position of followers by Eq. (3)
End if
Evaluate each salps fitness
Update the FoodPosition
End for
End While
Return FoodFitness
```

Next, as seen in Eq (4), Isaac Newton's theory of motion is used:

$$x_j^i = \frac{1}{2}k \times t^2 + s_0 \times t \tag{4}$$

Here, x_j^i signifies the i-th follower's position in the j-th dimension, t represents the iteration, s_0 represents the beginning speed, and k is defined in Equation (5):

$$k = \frac{s_{\text{final}}}{s_0} \tag{5}$$

With s_0 given in Equation (6)

$$s_0 = (x - x_0) \,/\, t \tag{6}$$

The steps of SSA and pseudocode are given in algorithm 1 in Table 1.

3. Proposed sine cosine mirror imaging chaotic perturbation-based Salp Swarm Algorithm (SCMSSA)

3.1. Logistic Chaotic Single-Dimensional Perturbation

Chaos is a state of disorder found in nonlinear dynamic systems and is prevalent in various natural and social circumstances [34]. Chaos exhibits qualities such as pseudo-randomness, ergodicity, and sensitivity to starting conditions. There are two types of chaotic systems: high-dimensional chaotic systems and one-dimensional chaotic systems. Logistic mapping is a very basic and extensively researched one-dimensional chaotic dynamic system that is defined as follows in equation (7) [35]:

$$C(t+1) = \mu C(t)(1 - C(t)) \tag{7}$$

Where the t-th chaotic sequence is represented by $C(t), 1 \leq t \leq (n-1)$. The parameter of the logistic chaotic sequence is $0 < \mu \leq 4$. The impact of various μ values on the chaotic distribution affects the sequence's ergodicity. The chaos parameter, $C(1)$ is randomly initialized from the range (0, 1) and ensures that $C(1)$ is not equal to 0.25, 0.5, 0.75, or 1. Movements made using chaos exhibit non-repeating behavior and offer greater search efficiency compared to random movements, as seen in Fig. 1b. As seen in Fig. 1b its values are uniformly distributed between 0 and 1, compared to Fig. 1a; therefore, discovering the best solutions in promising areas by using a one-dimensional chaotic traversal exploration is efficient. By using this method in SCMSSA, SCMSSA is able to find optimal solutions while maintaining the dimensional information associated with the ideal solution. This methodology was initially implemented by Ref. [36].This procedure is called the Logistic Chaotic Single-Dimensional Perturbation (LCSDP) [36].

The following is an expression for the LCSDP:

$$X(t+1) = X_{\text{best}} \tag{8}$$

$$X(t+1)i = lb_i + C(t)(ub_i - lb_i) \tag{9}$$

Here, lb_i and ub_i represent the lower boundary and upper boundary of the *ith* dimension. The LCSDP initially relocates the best solution's position to a novel position, $X(t+1),$ as defined in Eq. (8). Subsequently, utilizing Eq. (9), a dimension is chosen at random and $X(t+1)$ employs logistic chaos to investigate the search region in one dimension. It's worth noting that LCSDP is tailored to address the SCMSSA's limitation and greatly improve the algorithm's exploration capabilities. Most of the valuable dimensional information pertaining to the present best solution is preserved all through the search process, ensuring the algorithm's convergence towards the

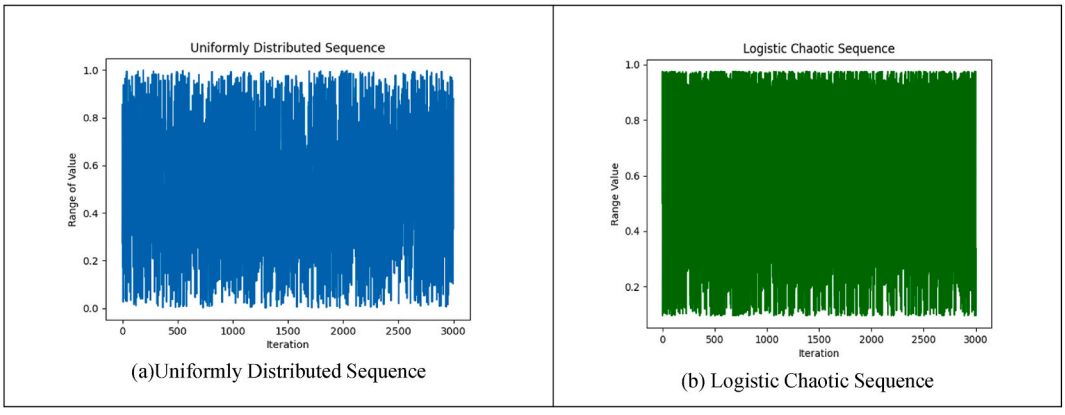

Fig. 1. Uniform and logisitic sequence [36].

optimal solution in a given problem. Conversely, this approach makes use of logistic chaos to continuously disrupt one dimension of the current best solution, boosting the algorithm's capacity to exit local optima in subsequent iterations.

3.2. Leveraging Convex Lens Imaging for Mirror Image Strategy

Opposition-Based Learning (OBL), pioneered by Tizhoosh, represents a notably efficient optimization methodology. It aims to expand the search space by computing opposing solutions based on existing ones. This approach culminates in the attainment of superior solutions for optimization conundrums [37]. One variant of OBL, known as the Lens imaging learning technique, is inspired by the principles of convex lens imaging in optics. This method produces better answers by using convex lenses that reflect items from one side to the opposite one. Yao et al. presented a new opposition-based learning technique referred to as the "mirror imaging strategy based on convex lens imaging, which is inspired by the idea of convex lens imaging and merged with the mirror imaging principle [38]. Employing the concept of mirror imaging, the methodology generates novel opposing solutions symmetrically to the inverse solution. By expanding the potential of convex lens imaging opposition solutions, this approach aids in navigating the optimization process away from local optima [38]. The application of this mechanism in our work is inspired by Ref. [38]. The mirror imaging strategy based on convex lens imaging, illustrated in Fig. 2, operates within a two-dimensional framework. The exploration of the solution space along the x-axis extends from LB (lower bound) to UB (upper bound). Along the y-axis, two distinct regions are delineated: the convex mirror area (depicted in blue) in the positive half-axis and the plane mirror area (shown in yellow) in the negative portion of the axis. When a salp (s) resides within the convex mirror region with a projection (X) on the x-axis within a height H, it undergoes convex lens imaging, resulting in the generation of a real image (s*) with a projection (X*) and a height H*. Subsequently, an opposition salp (s*) is derived. By employing the principle of plane mirror imaging, a new opposing individual (s**) is formed, featuring a projection (X**) and a height identical to H*, with $|X^{**}| = |X^{*}|$. Ultimately, the opposing salps (s*) and (s**) are generated based on the initial salp (s). The opposing point (s*) is determined concerning the individual (s), utilizing the origin of coordinates (O) as the reference point in alignment with the concept of convex lens imaging. The coordinates of this point can be calculated using Eq. (10).

$$\frac{(UB+LB)/2 - X}{X^{*} - (UB+LB)/2} = \frac{H}{H^{*}} \tag{10}$$

In the equation, UB represents the upper boundary, LB the lower boundary, and $\delta = \frac{H}{H^{*}}$. X^{*} defined in Equation (11)

$$X^{*} = \frac{UB+LB}{2} + \frac{UB+LB}{2\delta} - \frac{X}{\delta} \tag{11}$$

In lens imaging, the projection points along the x-axis through convex lens imaging exhibit variations contingent upon different lens thicknesses, where the thickness is defined as a dynamically adjustable value (scaling factor δ). This dynamic scaling factor facilitates the generation of a greater number of convex lens imaging solutions and consequently, more mirror imaging solutions. The scaling factor augments the local exploitation capability of the optimization algorithm. SCMSSA employs a nonlinear dynamic scaling factor strategy to accomplish these aims. During the initial iterations of the algorithm, substantial values may be attained, permitting the algorithm to extensively explore various dimensions, thereby enriching the diversity of the population. As the algorithm progresses, the attained values diminish, enabling more precise searches in the vicinity of the best search agent, thereby enhancing the algorithm's efficacy in local search. The calculation of the nonlinear dynamic scaling factor is delineated in Eq. (12):

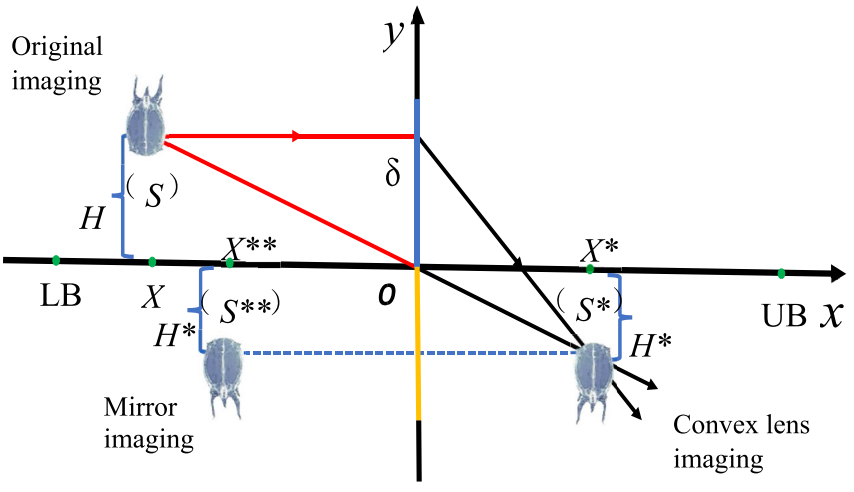

Fig. 2. Leveraging Convex Lens Imaging for Mirror Image Strategy [38] (Modified with permission from Elsevier, License Number 5764290728904).

$$\delta = \delta_{\max} \times \left[(\delta_{\max} - \delta_{\sin}) - 2 \times \left(\frac{t}{T}\right)^2 \right] \tag{12}$$

In this equation, $\delta_{\max}$ represents the upper limit for the scaling factor, $\delta_{\min}$ denotes the lower limit for the scaling factor, and T is the maximum number of iterations. Specifically, $\delta_{\max}$ is set to 10, and $\delta_{\min}$ to 9. Extending the concept presented in Eq. (11) to a k-dimensional space results in the following expression as in Equation (13).

$$X_k^* = \frac{UB_k + LB_k}{2} + \frac{UB_k + LB_k}{2\delta} - \frac{X_k}{\delta} \tag{13}$$

3.3. Combination of sine and cosine perturbations

The effectiveness and precision of the Salp swarm algorithm heavily depend on how the optimal individual's position is updated. This significant reliance on the optimal individual can hinder the algorithm's ability to find the global best solution, making it susceptible to local optima. To address this limitation, the paper introduces a combination of sine and cosine perturbations inspired by Ref. [38]. These perturbation factors are designed to enable the algorithm to escape local optima and enhance its ability to seek optimal solutions as shown in Equations (14) and (15):

$$\lambda_1 = 1 + \frac{1}{10000} \times (\sin(a \times 4\pi \times t) + \cos(a \times 6\pi \times t)) \times e^{\left(\frac{\pi}{100} \times \frac{T-t}{4}\right)} \tag{14}$$

$$\lambda_2 = 1 + \frac{1}{10000} \times (\cos(a \times 4\pi \times t) + \sin(a \times 6\pi \times t)) \times e^{\left(\frac{\pi}{100} \times \frac{T-t}{4}\right)} \tag{15}$$

The dynamic variations in sine and cosine disturbance factors introduce varying degrees of disruption to the position updates of salps, as illustrated in Fig. 3, allowing for a better exploration of the solution space. This expanded search scope enhances the algorithm's capacity to break free from the local optima.

The position update procedures once the disturbance factor has been introduced are displayed in the following Equations (16) and (17).

$$X_{i-cos}(t+1) = \lambda_1 \times X_i(t) + c_3 \times e^{-f_{\text{best}}^*/f_i} \times \text{rand}_i \times \left(FQ \times X_{\text{best}}^* - X_i(t)\right) \tag{16}$$

$$X_{i-sin}(t+1) = \lambda_2 \times X_i(t) + c_3 \times e^{-f_{\text{best}}^*/f_i} \times \text{rand}_i \times \left(FQ \times X_{\text{best}}^* - X_i(t)\right) \tag{17}$$

Where c_3 is a random number generated within [0,1], f_{best}^* denotes the fitness of the best salp, f_i represents the fitness value of the current salp, X_{best}^* is the current position of the best salp while FQ is given in Equation (18):

$$FQ = c_1 \times e^{(t-T)/T} \tag{18}$$

This strategy is combined into the SCMSSA strategy to escape local optimum and enhance searchability, the original SSA procedure in Eq. (3) is updated in SCMSSA as expressed in Equation (19):

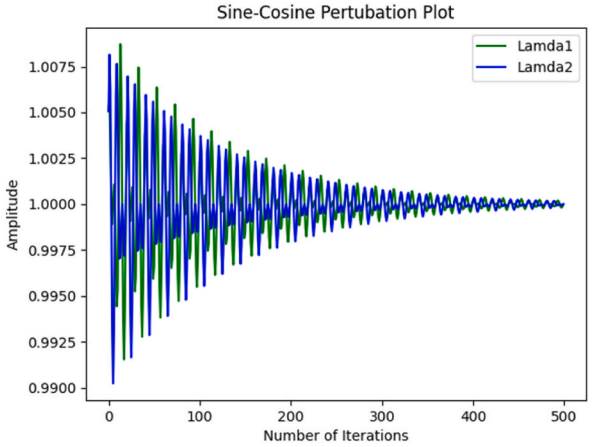

Fig. 3. Sine-Cosine Perturbation [38].

$$x_j^i = \frac{1}{2}\left(x_{j-sin}^i + x_{j-cos}^i\right) \tag{19}$$

3.4. SCMSSA improvement validation

Six distinct functions to assess the improvement of the SCMSSA algorithm are employed in this section. Notably, the selected functions consist of F1, F2, and F3, which can be categorized as single-peaked functions, and F4, F5, and F6, characterized as multipeaked functions are clearly detailed in Table 2 and graphically illustrated in Fig. 4, to show the complexity of each functions landscape. Furthermore, the SCMSSA algorithm was subjected to a comparative analysis alongside the Cuckoo Search(CS) [39], Grey Wolf Optimizer (GWO) [40], and SSA [41] with the primary aim of highlighting the search performance of the SCM algorithm. In order to ensure a fair and effective evaluation, both the maximum iteration number and the initial population size were consistently set at 500 and 30 for all algorithms. The parameter of each optimizer is given in Table 3.

The optimization performance of the algorithms is gauged using the average (AVG) and the Standard Deviation (STD) derived from 30 optimization results. This data is illustrated in Table 4 and Fig. 5, which provide insight into the optimization outcomes and convergence accuracy. The findings reveal that, when applied to single-peaked functions F1, F2, and F3, the SCMSSA algorithm demonstrates a mean value matching the optimal solution, and it exhibits swifter convergence compared to the SSA, CS and GWO algorithms. In the case of multipeaked functions F4, F5, and F6, the SCMSSA algorithm exhibits remarkable optimization performance, achieving near-ideal solutions when compared to its counterparts. The convergence curves depicted in Fig. 5 for all four algorithms indicate that the SCMSSA algorithm converges faster and more accurately toward the ideal or near-ideal optimal solution. Moreover, when dealing with challenging landscapes characterized by numerous local optima, such as in F3, F4, and F6, the SCMSSA algorithm surpasses its counterpart in terms of function optimization performance, convergence speed, and accuracy. To better understand the statistical significance of the proposed method. Friedman test, which is a non-parametric statistical test used to compare three or more paired groups, is employed in this research. As seen in Table 4, it's used to compare the performance of the four algorithms across all benchmark functions collectively rather than evaluating them separately on each function, unlike metrics like AVG and STD. These findings underscore the effectiveness of the algorithm enhancement discussed in this article. In Table 4, SCMSSA has the lowest Friedman rank sum (1.00), indicating it was the best performing algorithm across all benchmark functions on average, followed by GWO (2.33), SSA (3.00), and CS (3.67) being the least effective according to this test. The Friedman test is valuable because it provides a comprehensive statistical significance comparison across multiple test functions.

4. Co_2 prediction model based on SVR-SCMSSA

4.1. Support vector regression (SVR)

Vapnik proposed the support vector machine (SVM) in 1995 based on the statistical learning theory [42,43]. SVM generally aims to minimize classification error of test data. Because of this, SVM builds the best hyperplane for test data classification via the principle of structural minimization [43,44]. SVM can be divided into two classes: firstly, SVR, this type of support vector machine is a regression technique; secondly, support vector classification (SVC) which is a classification approach [45]. The SVR equation is seen in Equation (20):

$$f(x) = w \times \varphi(\mathrm{x}) + b \tag{20}$$

φ, b, and w, represent the mapping function, the intercept, and the weighted feature vector, respectively, while x represents the input vector to estimate the best value for b and w in Eq. (20), Eq. (21) is minimized:

$$\varphi(w, \varepsilon, \varepsilon^*) = \frac{1}{2}\| w\|^2 + C\sum_{i=1}^{1}(\varepsilon + \varepsilon^*) \tag{21}$$

Table 2
Benchmark functions.

Function	Range	Dim	Fmin
$f_1(x) = \sum_{i=1}^{n} x_i^2$	[-100,100]	50	0
$f_2(x) = \sum_{f_{min}}^{n} \lvert x_i\rvert + \prod_{i=1}^{n} \lvert x_i\rvert$	[-10,10]	50	0
$f_3(x) = \sum_{i=1}^{n}\left(\sum_{j-1}^{i} x_j\right)^2$	[-100,100]	50	0
$f_4(x) = \sum_{i=1}^{n} - x_i \sin\left(\sqrt{\lvert x_i\rvert}\right)$	[-500,500]	50	−418.9892 x dim
$f_5(x) = -20\exp\left(-0.2\sqrt{\frac{1}{n}\sum_{i=1}^{n} x_i^2}\right) - \exp\left((1/n)\sum_{i=1}^{n}\cos(2\pi x_i)\right) + 20 + e$	[-32,32]	50	0
$f_6(x) = \pi/n\left\{\sum_{i=1}^{n-1}(y_i-1)^2\left[1+10\sin^2(\pi y_{i+1})\right] + (y_n-1)^2\right\}$	[-50,50]	50	0
$+\sum_{i=1}^{n} u(x_i,10,100,4) + \pi/n10\sin(\pi y_1)y_i = 1 + x_i + (1/4)u(x_i,a,k,m) = \begin{cases} k(x_i-a)^m & x_i > a \\ 0 & -a < x_i < a \\ k(-x_i-a)^m & x_i < -a \end{cases}$			

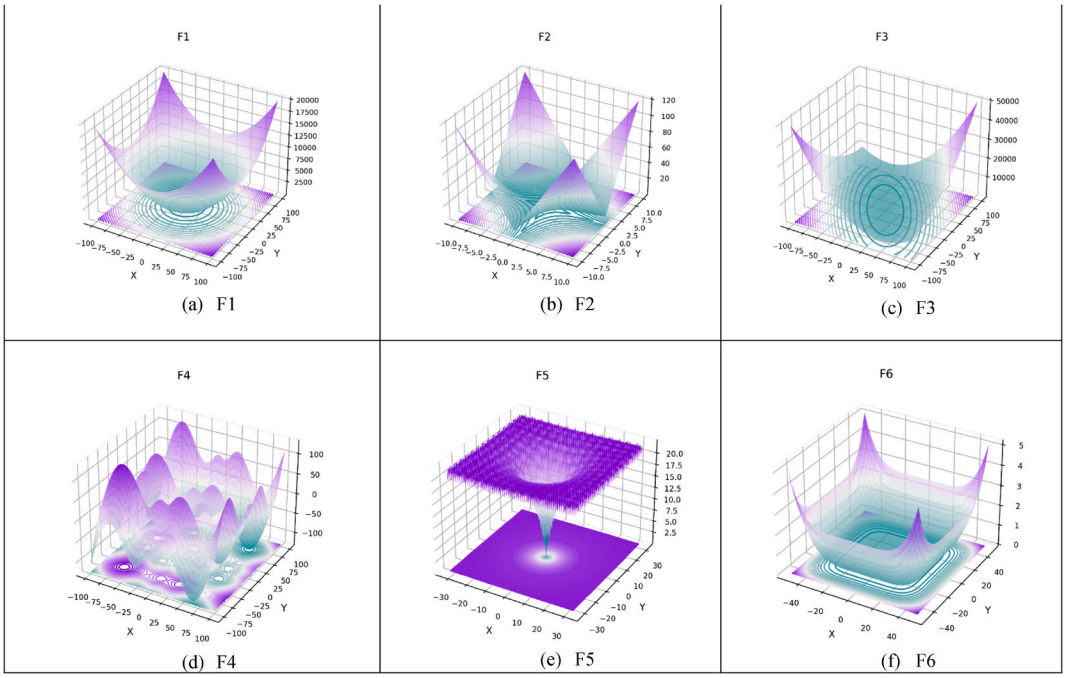

Fig. 4. 3D graph of benchmark functions F1 to F6.

Table 3
Parameter of optimizers.

Optimizer	Settings
CS	$Pa = 0.25, r = 0.05$
GWO	$a_0 = 2$
SSA	$c1 = [2/e, 2]$
SCMSSA	$c1 = [2/e, 2], a = 0.05$

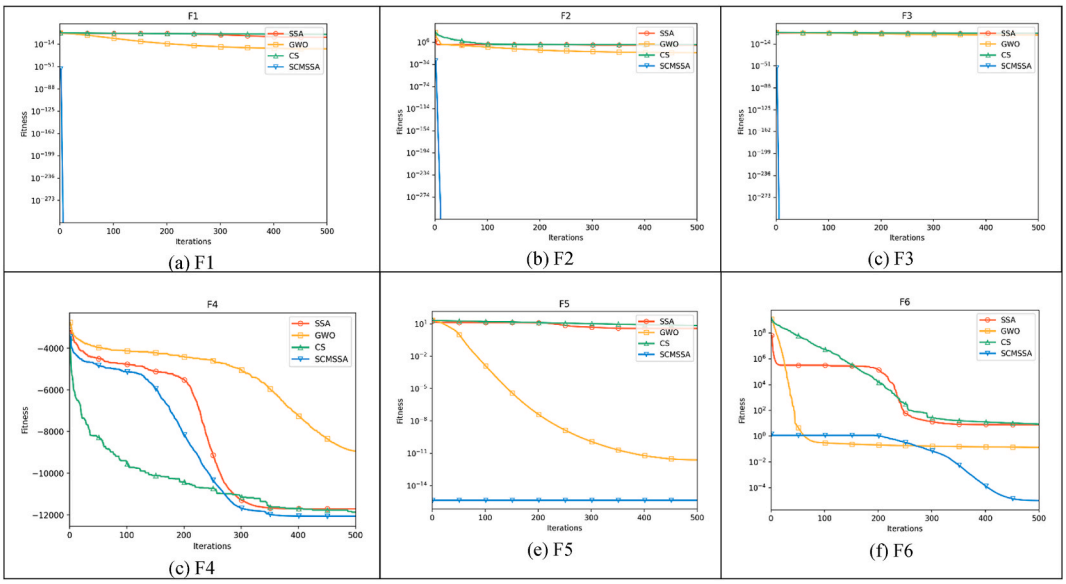

Fig. 5. Convergence curves of optimizers on benchmark functions F1 to F6.

Table 4
Benchmark function results of SCMSSA, SSA, CS and GWO.

		CS	GWO	SSA	SCMSSA
F1	AVG	2.645E+2	2.343E-22	2.884E-3	**0**
	STD	7.438E+1	2.216E-22	2.421E-3	**0**
F2	AVG	2.090E+1	1.016E-13	4.941	**0**
	STD	4.771	8.552E-14	2.391	**0**
F3	AVG	1.273E+4	4.309	4.829E+3	**0**
	STD	2.706E+3	4.105	2.820E+3	**0**
F4	AVG	−1.187E+4	−8.943E+3	−1.171E+4	**−1.207E+4**
	STD	1.385E+3	2.052E+3	**8.746E+2**	1.242E+3
F5	AVG	6.905	2.410E-12	3.792	**4.441E-16**
	STD	7.541E-1	1.370E-12	1.026	**0**
F6	AVG	8.386	1.303E-1	7.596	**9.800E-6**
	STD	1.496	9.249E-2	2.158	**9.359E-6**
	FRIEDMAN VALUE	3.67	2.33	3.00	1.00
	RANK	4	2	3	1

$\varepsilon, \varepsilon^{*,}$ and C respectively, depict two slack parameters and a penalty parameter. Based on the condition given in Eq. (22), Eq. (21) is minimized.

$$\begin{cases} \mathrm{y_i} - \mathrm{w} \cdot \varphi(\mathrm{x}) - \mathrm{b} \leq \varepsilon + \varepsilon_\mathrm{i} \; \varepsilon_\mathrm{i} \geq 0 \\ \mathrm{w} \cdot \varphi(\mathrm{x}) + \mathrm{b} - \mathrm{y_i} \leq \varepsilon + \varepsilon_\mathrm{i}^* \; \varepsilon_\mathrm{i}^* \geq 0 \end{cases} \tag{22}$$

$\mathrm{y_i}$ represents the actual output vector. The slack parameters, as seen in Eq. (22), measure the error of each equation as seen in Fig. 6, Eqs. (21) and (22) becomes an optimization problem. This problem can be solved by using the Lagrangian equation in Eq. (23):

$$f(x) = \sum_{i=1}^{N} (\alpha_i - \alpha_i^*) K(x, x_i) + b \tag{23}$$

$K(x, x_i)$ represents a kernel function, the Lagrangian multipliers are represented by α_i^* and α_i. The Lagrangian multipliers and penalty are greater than 0. The kernel function is used to resolve the challenge of nonlinearity in the input data, the kernel function projects the input data to a feature space with high dimension [43,46]. There are many types of kernel functions Gaussian basis, sigmoid, linear, and radial basis.

The Radial Basis is given in Equation (24):

$$\mathrm{K}(x, x_i) = \exp\left(- \parallel x - x_i \parallel \; / 2\sigma^2\right) = \exp\left(-\gamma \parallel x - x_i \parallel^2\right) \tag{24}$$

The Sigmoid is given in Equation (25):

$$\mathrm{K}(x, x_i) = \tanh\left(\mathrm{k}(x.x_i) + \mathrm{v}\right), \mathrm{k} > 0, \mathrm{v} < 0 \tag{25}$$

Gaussian Basis is given in Equation (26):

$$\mathrm{K}(x, x_i) = (1 + x.x_i)^{\mathrm{d}} \tag{26}$$

Deciding the best kernel function and C are the important hyper-parameters that directly affect the performance of SVR. These

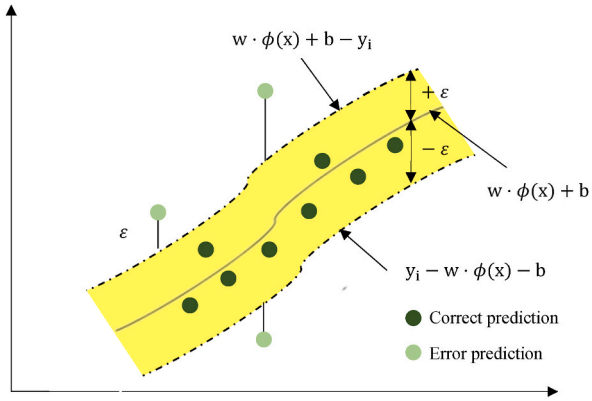

Fig. 6. Support vector Regression Illustration.

parameters are the γ value in the radial basis kernel function $K(x, x_i)$ and the penalty parameter C. They are intimately tied to SVR's predictive capabilities and its ability to generalize. Consequently, it becomes imperative to employ an optimization algorithm for fine-tuning SVR's hyperparameters. The pseudo-code for SVR-SCMSSA is presented in Algorithm 2 in Table 5.

4.2. Building CO_2 prediction model

Predicting CO_2 levels represents a classic challenge characterized by high dimensionality and nonlinearity. The SVR approach leverages kernel functions to transform sample data from a lower-dimensional space to a higher-dimensional one, thereby facilitating finding the solution to this complex problem. The accuracy of CO_2 prediction using SVR is notably influenced by the parameters C and $K(x,x_i)$, as outlined in Eqs. (21) and (23). SVR relies on these key components to achieve accurate predictions. One of these components is the Penalty C, this hyper-parameter dictates the trade-off between minimizing training error and reducing testing error. By adjusting C, one can control the width of the margin around the regression line. A small C value leads to a wider margin, potentially ignoring some training points and causing underfitting, characterized by high bias and low variance. Conversely, a large C tightens the margin, striving to fit the training data more closely but risking overfitting with low bias and high variance. Therefore, tuning the C parameter is vital to strike the right balance and enhance the model's accuracy while ensuring it generalizes well to unseen data. Another critical element in SVR is the selection of the appropriate Kernel function $K(x,x_i)$, which maps input data from the original feature space to a higher-dimensional space, enabling effective regression. The choice of Kernel function, such as Linear, Radial Basis Function (RBF), or Polynomial, depends on the data's inherent relationships and complexities. Each kernel has its associated hyperparameters (e.g., γ for RBF) that significantly affect the model's accuracy. Therefore, careful consideration of both the Penalty C and the choice of Kernel function $K(x, x_i)$, along with their respective hyperparameters, is paramount for optimizing SVR and achieving precise predictions tailored to the specific problem at hand. To improve the predictive accuracy of the SVR model for CO_2 prediction, this study employs the SCMSSA algorithm to determine optimal values for the hyper-parameters C and $K(x, x_i)$. The choice of Sine Cosine perturbation, Chaotic perturbation, and Mirror imaging strategy as enhancement mechanisms is grounded in their ability to address specific limitations of the original Salp Swarm Algorithm (SSA) and to improve the overall performance of the Support Vector Regression (SVR) model for CO2 prediction. Sine Cosine Perturbation, The sine and cosine functions offer a mathematical model to diversify the trajectory of the salps, allowing them to search in an oscillatory pattern, which is effective in navigating both local and global search spaces. In the Chaotic Perturbation, chaotic systems are sensitive to initial conditions and have been observed to exhibit non-repeating, complex patterns over time. Applying chaos theory to optimization, specifically through chaotic maps such as the logistic map,

Table 5
Algorithm 2: Pseudocode SVR-SCMSSA

```
Input: Dataset, Maximum Number of Iterations, Number of Salps
First Stage:
Split data into two parts (training and testing)
Initialize the population randomly.
Compute the fitness of each individual in the population (SVR Fitness Function)
Sort the fitness values and set FoodFitness as the best salp's fitness and
Food Position is set as the best salp's position
Second Stage:
while t ≤ T do
Compute r1 using Eq. (2)
For (Each Salp):
If i ≤ N/2 do
Update each individual position using Eq. (1)
Else
/* Sin-Cosine Perturbation*/
Update each individual position using Eq. (19)
End if
/* Chaotic Perturbation*/
Generate new Salp position X_new using Eq. (9)
If fitness(X_new) < Fitness(X_currentsalp):
X_currentsalp = X_new,
End if
/* Mirror Imaging Strategy*/
Generate new Salp position X_new using Eq. (13)
If fitness(X_new) < Fitness(X_currentsalp):
X_currentsalp = X_new,
End if
Update FoodFitness and FoodPosition
End for
End while Stop criteria satisfied.
Return FoodPosition
Third Stage:
Use FoodPosition to Train the SVR model
Test the SVR model with training data
Evaluate the SVR model using different metrics
```

introduces controlled randomness that enhances the algorithm's exploration capabilities. Mirror Imaging Strategy, this method is grounded in the concept of opposition-based learning, where considering opposite or complementary solutions can lead to faster convergence to the global optimum by simultaneously exploring and exploiting different regions of the search space. Fig. 7 illustrates the predictive process for CO_2 using SVR-SCMSSA, and the following procedures:

Step 1 Initiate by importing the input features associated with CO_2 generation and the corresponding CO_2 output. After normalizing the data, partition it into separate training and test sets.
Step 2 Specify a parameter optimization range (C and $K(x,x_i)$) for the SVR model. Proceed to train the SVR model using the provided training dataset.
Step 3 Commence by initializing the parameters of the SCMSSA algorithm and generating the initial population of Salps within the predefined parameter range.
Step 4 Determine the fitness value for each Salp through the SVR model, utilizing the Root Mean Square Error(RMSE) as the fitness function. Identify the most exceptional Salp as "FoodFitness" and document its position as "FoodPosition."

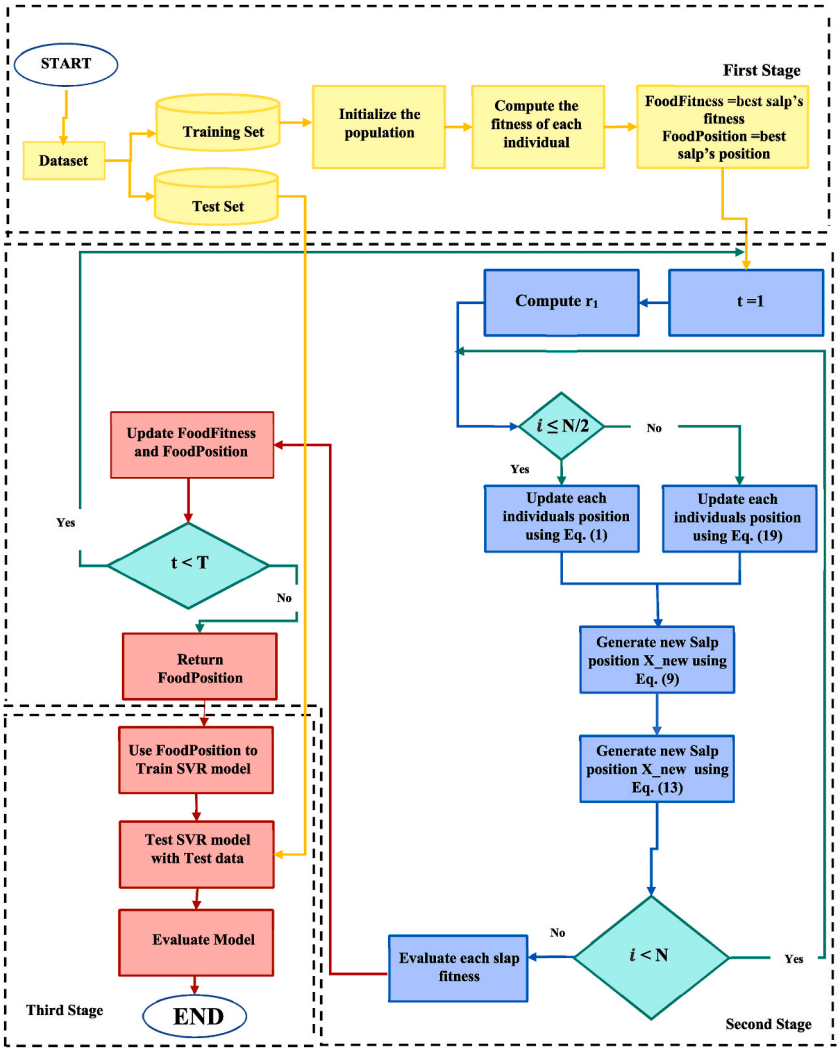

Fig. 7. Flow chart of SVR-SCMSSA

Step 8 Ascertain whether the present iteration reaches the maximum allowable iteration limit. If so, provide the best values for C and the kernel function obtained from the most exceptional salp. Alternatively, revert to step 4.
Step 9 Construct the SVR-SCMSSA model using the optimal C and kernel function obtained by SCMSSA.
Step 10 Validate the predictive model by testing it with the test dataset.
Step 11 Assess the model's performance utilizing a range of evaluation metrics.

Step 5 Calculate r_1, and for each Salp, if the number of Salps is less than the population size divided by 2, update their positions employing the SSA operator expressed in Eq. (1). In cases where this condition doesn't apply, make adjustments using Sine Cosine perturbation expressed in Eq. (19).

Step 6 Create fresh positions for each Salp through Chaotic Perturbation as given in Eq. (9). Accept these newly generated positions only if their fitness is better than that of the current positions.

Step 7 Employ a Mirror Imaging strategy to establish new positions for each Salp as given in Eq. (13). Keep these new positions if they yield superior fitness compared to the current ones. Update "FoodPosition" and "FoodFitness" accordingly.

These stages delineate the process of utilizing the SCMSSA algorithm to enhance the SVR model for precise CO_2 prediction, incorporating diverse strategies to ameliorate the model's efficacy and predictive accuracy.

4.3. Fitness function and evaluation metrics

A collection of evaluation measures, including Mean Square Error (MSE), Mean Absolute Percentage Error (MAPE), Mean Absolute Error (MAE), Root Mean Square Error (RMSE), and the Coefficient of Determination (R^2), are used in this article to evaluate the performance of the SVR models. The mathematical formulation of these metrics is given in Eq. 27–30. Every SVR model uses the RMSE metric as its fitness function to assess how well each algorithm performs.

$$MAE = \frac{1}{n}\sum_{i=1}^{n} \left| \mathscr{Y}_i - \mathscr{Y}_i^* \right| \tag{27}$$

$$MSE = \frac{1}{n}\sum_{i=1}^{n} \left(\mathscr{Y}_i - \mathscr{Y}_i^* \right)^2 \tag{28}$$

$$\mathrm{MAPE} = \frac{1}{n}\sum_{i=1}^{n} \left| \frac{\mathscr{Y}_i - \mathscr{Y}_i^*}{\mathscr{Y}_i} \right| \tag{29}$$

$$R^2 = 1 - \frac{\sum_{i=1}^{n} \left(\mathscr{Y}_i - \mathscr{Y}_i^* \right)^2}{\sum_{i=1}^{n} \left(\mathscr{Y}_i - \bar{y} \right)^2} \tag{30}$$

Where $\mathscr{Y}_i$ represents the actual value of CO_2, $\bar{y}$ represents the mean of the actual value of CO_2, $\mathscr{Y}_i^*$ represents the predicted value of CO_2 and n is the number of data points in the dataset.

5. Data description and processing

This study utilizes data obtained from the U.S. Energy Information Administration, encompassing 605 data points gathered between January 1973 and May 2023, focusing on CO_2 generation from energy consumption. To account for variations in the magnitudes of different factors, the sample data undergo normalization, thereby mitigating the influence of magnitudes across various factors. Subsequently, the sample data is partitioned into test and training samples, following a ratio of 3:7. A normalized mathematical representation is depicted in Eq. (31):

$$x_{\mathrm{new}i} = \frac{x_i - x_{min}}{x_{max} - x_{min}} \tag{31}$$

$x_{\mathrm{new}i}$ represents the normalized figure, x_i stands for the original value, while x_{max} and x_{min} indicate the highest and lowest values, respectively. The first 10 entries of the normalized dataset are illustrated in Table 6. Also, variables in Table 6 are CO_2 (Carbon Dioxide), Fossil (Fossil Fuels: which include coal, oil, and natural gas), Nuclear (Nuclear Energy), Hydro (Hydroelectric Power: Energy generated from water), Geothermal (Geothermal Energy: Energy derived from the Earth's internal heat), Wood (Energy from burning or converting wood), Waste (Waste-to-Energy: Energy generated from the incineration of waste materials), Biomass (Biomass Energy:

Table 6
Sample of normalized data.

S/N	Duration	CO2	Fossil	Nuclear	Hydro	Geothermal	Wood	Waste	Biomass
1	1973 January	0.653004	0.653683	0.036389	0.733678	0.033904	0.153554	0.091677	0.087484
2	1973 February	0.505440	0.481460	0.015732	0.616859	0.000000	0.025820	0.078254	0.014859
3	1973 March	0.474761	0.444577	0.061076	0.719518	0.013341	0.154853	0.109418	0.088322
4	1973 April	0.308360	0.262757	0.012269	0.660545	0.071949	0.112162	0.107643	0.064073
5	1973 May	0.342921	0.303953	0.000000	0.689614	0.045381	0.153495	0.136846	0.087745
6	1973 June	0.271232	0.211663	0.069029	0.647522	0.097198	0.111889	0.109418	0.063929
7	1973 July	0.315311	0.266687	0.079165	0.589947	0.119252	0.153417	0.104031	0.087484
8	1973 August	0.383101	0.349227	0.123412	0.531443	0.096984	0.154569	0.116321	0.088211
9	1973 September	0.277395	0.222050	0.127308	0.323109	0.034157	0.113585	0.111172	0.064909
10	1973 October	0.383348	0.354649	0.109620	0.386706	0.096555	0.154911	0.129270	0.088499

Energy produced from organic materials like plant matter or agricultural waste). The correlation between features in the data can be seen in Fig. 8, the correlation between features in data" refers to how two or more variables relate to each other. It can be positive (both go up), negative (one goes up, the other down), or no correlation (no clear relationship). Understanding these relationships is essential for data analysis and modelling.

6. Results and discussion

The four SVR-based hybrid models, SVR and Extreme Learning Machine (ELM), in this study, are trained using the training dataset. Fig. 9 displays an analysis of the correlation between the predicted and actual values in the training dataset. It is evident that the hybrid models exhibit relatively favourable training performance, with the training data points closely distributed around the ideal fitting line, "actual value = predictive value." When considering the R^2, the SVR-SCMSSA hybrid model stands out with a superior training performance, achieving an R^2 value of 0.95862. In comparison, the training performance of the SVR-SSA hybrid model and SVR are slightly less, with R^2 values of 0.91739 and 0.91585, respectively. Hybrid Models, such as SVR-SCMSSA, SVR-CS, and SVR-SSA, exhibit R^2 values predominantly above 0.90 in Table 7. Notably, SVR-SCMSSA reaches an impressive 0.95865, underscoring the considerable training achievements of the hybrid model introduced in this research.

Upon completing the model training, the four SVR-based hybrid models, the SVR and ELM model, undergo verification and evaluation using the testing dataset. In Fig. 10, the analysis of the correlation between predicted values and actual values in the testing dataset reveals that the testing data points also cluster around the ideal fitting line, "actual value = predictive value." Evaluating the prediction performance using the R^2 score metric, the proposed SVR-SCMSSA hybrid model achieves a score of 0.95775. This indicates that the hybrid models demonstrate a significantly higher level of prediction accuracy in comparison to their counterparts, such as SVR-CS and SVR-SSA hybrid models, which exhibit prediction accuracies of 0.9291 and 0.92887, respectively in Table 8. The computational efficiency of an optimization algorithm like SCMSSA refers to its ability to find optimal or near-optimal solutions within a reasonable time frame and with minimal computational resource usage. This efficiency is crucial when dealing with large-scale datasets or models requiring extensive parameter tuning, such as SVR models for CO2 prediction. The SCMSSA algorithm improves computational efficiency through several key aspects. Firstly, by integrating Sine Cosine perturbation, Chaotic perturbation, and Mirror imaging strategy, SCMSSA is able to avoid premature convergence and explore the solution space more effectively. This reduces the number of iterations needed to reach an optimal solution, directly impacting the computational time positively as in Tables 7 and 8, SCMSSA achieved optimal results within specified iteration number compared to other models. Lastly, the strategic perturbations in SCMSSA minimize the need for extensive computations in each iteration by focusing the search around promising areas of the solution space. This approach requires fewer function evaluations compared to brute-force or exhaustive search methods, reducing the overall computational load. Furthermore, Scalability refers to the algorithm's ability to maintain its performance and efficiency as the size of the dataset or the complexity of the problem increases. SCMSSA's scalability is supported by several factors. (1) The adaptive nature of the perturbation mechanisms in SCMSSA allows the algorithm to adjust its search strategy based on the problem's complexity. This adaptability ensures that SCMSSA can handle larger datasets or more complex prediction models without a significant increase in computational time or resource requirements. (2) The mirror imaging strategy and chaotic perturbation enhance the algorithm's capability to navigate high-dimensional solution spaces effectively. This is particularly important for SVR models, which may involve multiple hyperparameters and complex feature interactions, ensuring SCMSSA's scalability in these scenarios.

To conduct a more in-depth comparison and assessment of the prediction capabilities of the hybrid models, the performance of each hybrid model is compiled in Tables 7 and 8 The analysis reveals that the SVR-SCMSSA hybrid model outperforms the other hybrid models and the standard SVR, both on the training dataset and the testing dataset. This observation indicates that the improvement techniques introduced in the SVR-SCMSSA hybrid model significantly enhance the optimization of the algorithm for tackling complex problems. Moreover, it exhibits swift convergence, high precision, and robust resistance to falling into local optima, all of which

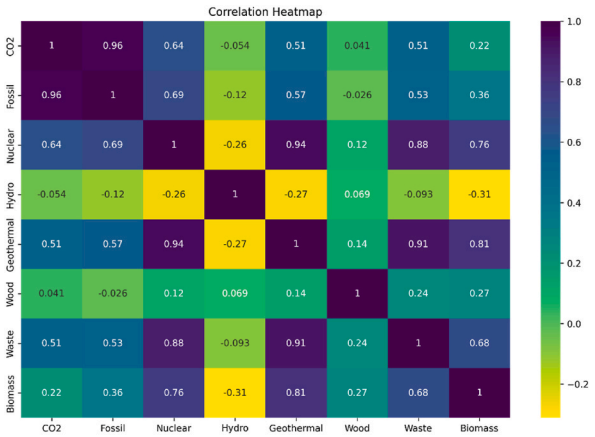

Fig. 8. Correlation Plot of data features.

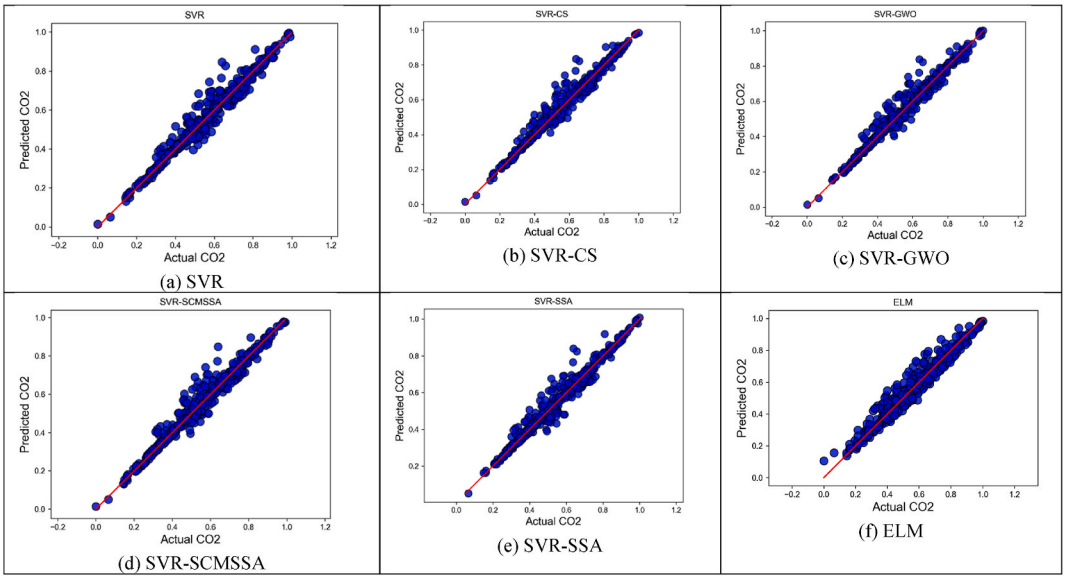

Fig. 9. Training Actual vs Prediction of Optimizer tuned SVR models ELM model.

Table 7
Result of evaluation metrics for training.

	RMSE	R^2	MSE	MAE	MAPE
SVR-GWO	0.00122	0.89657	0.00126	0.03081	0.50773
SVR-SCMSSA	0.00079	0.95862	0.00055	0.01683	0.27855
SVR-CS	0.00105	0.90531	0.00114	0.02567	0.42398
SVR-SSA	0.00080	0.91739	0.00087	0.02090	0.34563
SVR	0.00084	0.91585	0.00102	0.01951	0.32274
ELM	0.04365	0.94768	0.00191	0.03212	0.70330

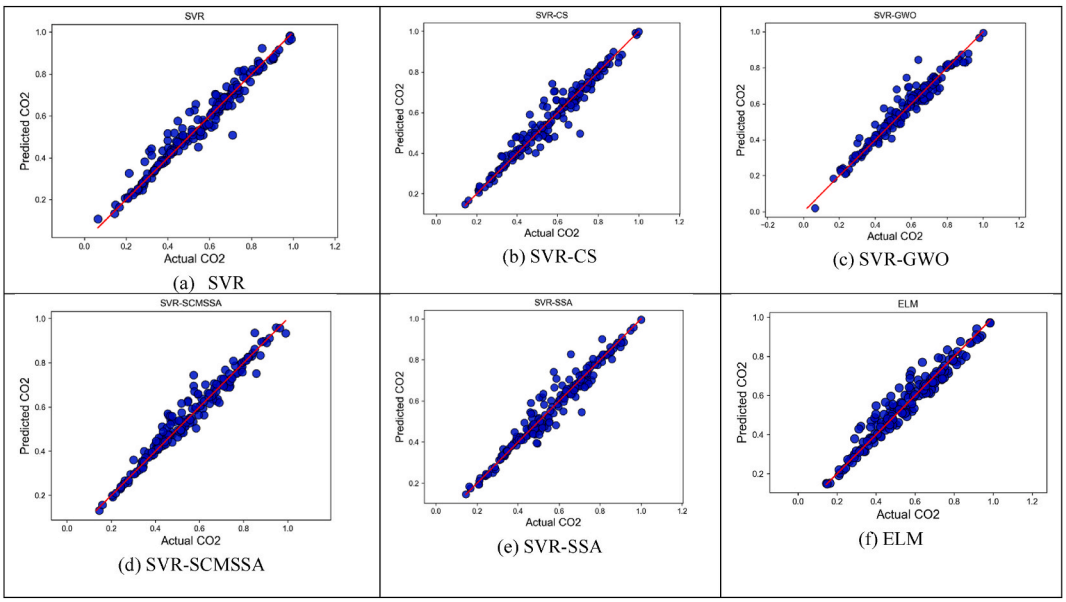

Fig. 10. Testing Actual vs Prediction Optimizer tuned SVR models ELM model.

Table 8
Result of evaluation metrics for testing.

	RMSE	R^2	MSE	MAE	MAPE
SVR-GWO	0.00137	0.89660	0.00137	0.03237	0.53437
SVR-SCMSSA	0.00056	0.95775	0.00056	0.01634	0.26985
SVR-CS	0.00093	0.92961	0.00093	0.02247	0.37170
SVR-SSA	0.00094	0.92887	0.00094	0.02171	0.35921
SVR	0.00133	0.89983	0.00133	0.03154	0.52002
ELM	0.04934	0.92862	0.00243	0.03520	0. 27657

surpass the capabilities of the traditional SSA algorithm. Fig. 11 demonstrates a comparison between the predicted and actual values of the testing dataset using the SVR-SCMSSA hybrid model. The predictive values closely align with the actual values, underscoring the model's superior learning and prediction prowess. Therefore, this paper recommends the utilization of the SVR-SCMSSA hybrid model researchers and Policy Makers for CO_2 prediction.

SCMSSA stands out due to its novel integration of enhancement mechanisms that address common optimization challenges such as premature convergence, the balance between exploration and exploitation, and navigating complex landscapes. Unlike traditional methods that might struggle with either becoming stuck in local optima or inefficiently searching the solution space in optimizing SVR for CO2 prediction, SCMSSA's sine cosine perturbation allows for a fluid transition between exploration and exploitation, enhancing the search process. The addition of chaotic perturbation prevents premature convergence by introducing randomness, thereby aiding in navigating complex parameter spaces more effectively.

6.1. Significance of study: insight into relative influence of features and limitations of study

In this session, we embark on a comprehensive analysis to assess the relative importance of each feature within our dataset. The features used in this research were chosen by identifying potential predictors of CO2 emissions, including energy consumption types (Fossil, Nuclear, Hydro, Geothermal), renewable sources (Wood, Waste, Biomass), and other relevant environmental or economic factors. This process was guided by domain knowledge and a literature review to ensure all significant contributors to CO2 emissions were considered. The significance of this assessment cannot be overstated, as it plays a pivotal role in our pursuit of sustainability. The key technique we employed in this endeavour is SVR-SCMSSA, an optimization algorithm that fine-tunes the parameters of SVR. By optimizing these parameters, SVR can then learn to make more accurate predictions, particularly regarding CO_2 emissions, making it an essential tool for sustainable decision-making. Understanding the relative influence of features on CO_2 prediction is of paramount importance. This knowledge enables us to identify which variables have the most substantial impact on our predictions. For example, it might shed light on whether "Nuclear" or "Geothermal" energy sources have a more significant effect on CO_2 predictions, offering crucial insights for energy and environmental policymakers. This information not only enhances our model's performance but also holds the potential to drive data-driven decisions in the realm of sustainability. By pinpointing the most influential factors, we can develop more effective strategies for reducing carbon emissions, transitioning to cleaner energy sources, and ultimately contributing to a greener and more sustainable future.

As depicted in Fig. 12, the analysis of variable importance concerning CO_2 reveals that fossil fuels stand out as the most influential factor. The importance score, which is the permutation importance score assigned to each feature by the SVR-SCMSSA model assigned to fossil fuels, is impressively above 1.4, indicating a robust and strong impact on the prediction of CO_2. This prominence can be attributed to the well-established fact that the combustion of fossil fuels is a primary source of CO2 emissions [47,48], making it a pivotal contributor. In addition to fossil fuels, Biomass, and Wood are other noteworthy variables displaying significant sensitivity. This result highlights the importance of Biomass and Wood as a factor impacting CO_2 emissions. Other studies validate the positive and negative impact of Biomass on CO_2 generation [49,50], which could be due to combustion processes involving Biomass fuels and Wood. Consequently, when constructing CO_2 prediction models, it is imperative to place substantial emphasis on the role of fossil fuels. Their strong correlation and well-established connection to CO_2 emissions underscore their critical importance. Moreover, the sensitivity of Biomass fuels, as indicated by its importance score also suggests that it should not be overlooked in the design of these models. Ultimately, these findings emphasize the necessity of considering these factors when aiming to develop accurate and effective CO_2 prediction models, which are vital for addressing environmental sustainability and climate change mitigation.

SVR-SCMSSA is tuned for the specific dataset in this study, and its effectiveness is intricately tied to the characteristics and distribution of the data. While it may yield promising results for the current dataset, it may not be a suitable choice for all scenarios. The model's performance hinges on the underlying data and the hyperparameter of SVR-SCMSSA. As the relationships between the features and the target variable change, such as the emergence of non-linear associations between certain features and CO_2 levels, adapting the SVR-SCMSSA algorithm becomes necessary. In these cases, selecting a different kernel function or adjusting other hyperparameters of the SVR model might be more appropriate. This necessitates an iterative process of fine-tuning to ensure the model can effectively capture the evolving data dynamics. It's important to note that SVR-SCMSSA can be computationally demanding. The optimization process may require substantial computational resources, which can be a limitation, particularly for large datasets or in scenarios where computational efficiency is crucial. Based on our model's findings, we suggest the following policy interventions and mitigation strategies.

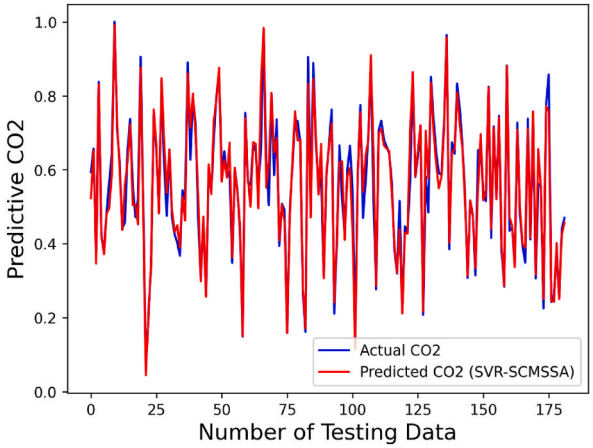

Fig. 11. Testing Actual vs Prediction.

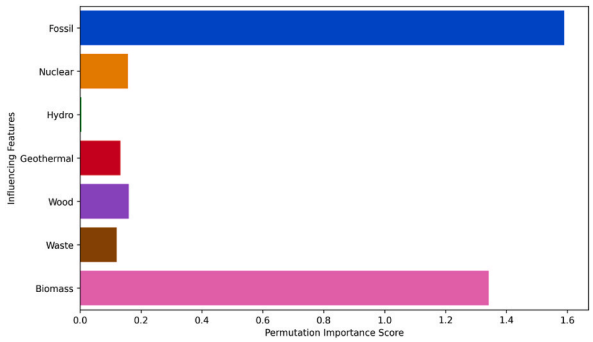

Fig. 12. Permutation Importance Score of the SVR-SCMSSA model.

1. Enhanced Renewable Energy Adoption: Given the substantial contribution of fossil fuel consumption to CO2 emissions, a key policy recommendation is to accelerate the transition towards renewable energy sources. Governments can support this transition through subsidies for renewable energy projects, tax incentives for clean energy investments, and stricter regulations on fossil fuel emissions.
2. Energy Efficiency Improvements: Our model underscores the importance of energy efficiency in mitigating CO2 emissions, given that the most contributing factors are majorly energy sources. Policy measures could include setting higher energy efficiency standards for buildings and appliances, promoting energy-saving technologies, and implementing national energy efficiency awareness campaigns.
3. Industrial Emission Controls: For industrial activities identified as major CO2 contributors, implementing stricter emission standards and investing in cleaner production technologies are critical. Policies could focus on carbon capture and storage (CCS) technologies, waste heat recovery systems, and the promotion of circular economy principles to reduce industrial carbon footprints.
4. Carbon Pricing Mechanisms: Introducing or enhancing carbon pricing mechanisms, such as carbon taxes or cap-and-trade systems, can provide financial incentives for reducing CO2 emissions. These mechanisms make it more cost-effective for businesses and individuals to adopt lower-carbon practices.
5. Afforestation and Reforestation Initiatives: Since forests play a crucial role in sequestering CO2, policies supporting afforestation and reforestation can contribute to offsetting emissions. This can include grants for tree planting projects, protection of existing forests, and sustainable land management practices.

By integrating these policy interventions and mitigation strategies into national and international climate action plans, policymakers can leverage the insights provided by our model to make informed decisions aimed at reducing CO2 emissions and combating climate change.

7. Conclusion

In this study, we proposed an improved Salp Swarm Algorithm that utilizes three improvement mechanisms to enhance the convergence accuracy and speed by tackling limitations in the exploration and exploitation of the original SSA. The improved SCMSSA

algorithm was compared to other algorithms on six test functions to validate the improvement. The SCMSSA algorithm was then employed as an optimization strategy for the SVR model, the result demonstrates the efficacy of the SVR-SCMSSA hybrid model in optimizing SVR for CO_2 prediction. The training and testing analyses revealed that SVR-SCMSSA outperforms other hybrid models and the standard SVR, achieving higher training and prediction accuracy. Its swift convergence, precision, and resistance to local optima make it a superior choice for tackling complex problems in CO_2 prediction. Therefore, this paper recommends the utilization of the SVR-SCMSSA hybrid model for more accurate and reliable CO_2 prediction, which is crucial for sustainability efforts. Additionally, the feature importance analysis provided valuable insights into the key contributors to CO_2 prediction. These findings highlight the importance of certain key factors such as Fossil Fuel, Biomass, and Wood when developing CO_2 prediction models, which is essential for addressing environmental sustainability and mitigating climate change.

Future work in this research area will focus on enhancing the generalizability of the SVR-SCMSSA hybrid model, assessing its performance on diverse datasets to determine its broader applicability. Extending our research to include a wider range of datasets that encompass different environmental, economic, and social contexts. This expansion will enable us to assess the robustness of the SVR-SCMSSA hybrid model across various scenarios, further solidifying its applicability for CO2 prediction globally. Furthermore, research efforts will be directed towards addressing the adaptability of the model to dynamic feature relationships, particularly in the presence of non-linear associations, through dynamic kernel selection and automated hyper-parameter tuning. It is also crucial to explore methods for improving the computational efficiency of SVR-SCMSSA to make it more accessible for use on larger datasets, potentially through parallelization and more efficient optimization algorithms. Future work will also delve deeper into the parameter tuning aspect, providing detailed guidelines and recommendations for practitioners aiming to apply the SVR-SCMSSA model to varied datasets. By doing so, we aim to enhance the model's adaptability and ease of use, further contributing to its practical application in the field of CO2 prediction and beyond. Additionally, investigating techniques to incorporate inter-feature dependencies into the optimization process would be essential for capturing feature interactions and enhancing the model's predictive capabilities. Furthermore, we will examine Model Adaptation for Long-Term Prediction, Scenario Analysis that evaluates the model's performance under future emission scenarios, and a sensitivity analysis to identify which parameters and assumptions have the most significant impact on long-term CO2 predictions. In summary, future research should aim to make SVR-SCMSSA a more versatile and efficient tool for CO2 prediction and feature importance analysis, broadening its applicability in a variety of scenarios. Finally, an open challenge in CO2 prediction is the difficulty in accounting for unexpected emission sources and the rapid changes in environmental policies. These challenges underscore the complexity of accurately forecasting CO2 emissions, where unforeseen technological advancements, shifts in global energy markets, or sudden policy implementations can significantly alter emission trajectories. Addressing these challenges calls for dynamic models that can quickly adapt to new information and incorporate a broader range of predictive variables, including potential indicators of policy shifts and emerging emission sources. Future research could focus on developing more agile and adaptive modelling approaches, possibly leveraging real-time data streams and advanced machine learning techniques capable of updating predictions in response to new developments.

The data obtained through the experiments are available upon request.

CRediT authorship contribution statement

Oluwatayomi Rereloluwa Adegboye: Writing – original draft, Investigation, Conceptualization. **Afi Kekeli Feda:** Resources, Formal analysis, Data curation. **Ephraim Bonah Agyekum:** Validation, Resources, Methodology. **Wulfran Fendzi Mbasso:** Writing – review & editing, Methodology. **Salah Kamel:** Writing – review & editing, Visualization, Formal analysis.

Declaration of competing interest

The authors declare that they have no known competing financial interests or personal relationships that could have appeared to influence the work reported in this paper.

References

[1] Intergovernmental Panel on Climate Change (IPCC), Climate Change 2021 – the Physical Science Basis: Working Group I Contribution to the Sixth Assessment Report of the Intergovernmental Panel on Climate Change, Cambridge University Press, Cambridge, 2023, https://doi.org/10.1017/9781009157896.

[2] J.L. Holechek, H.M.E. Geli, M.N. Sawalhah, R. Valdez, A global assessment: can renewable energy replace fossil fuels by 2050? Sustainability 14 (2022) 4792, https://doi.org/10.3390/su14084792.

[3] M.A. Abbasi, S. Parveen, S. Khan, M.A. Kamal, Urbanization and energy consumption effects on carbon dioxide emissions: evidence from Asian-8 countries using panel data analysis, Environ. Sci. Pollut. Res. 27 (2020) 18029–18043, https://doi.org/10.1007/s11356-020-08262-w.

[4] O.A. Osobajo, A. Otitoju, M.A. Otitoju, A. Oke, The impact of energy consumption and economic growth on carbon dioxide emissions, Sustainability 12 (2020) 7965, https://doi.org/10.3390/su12197965.

[5] K.O. Yoro, M.O. Daramola, Chapter 1 - CO2 emission sources, greenhouse gases, and the global warming effect, in: M.R. Rahimpour, M. Farsi, M.A. Makarem (Eds.), Adv. Carbon Capture, Woodhead Publishing, 2020, pp. 3–28, https://doi.org/10.1016/B978-0-12-819657-1.00001-3.

[6] M. Umar, A.A. Awosusi, O.R. Adegboye, O.S. Ojekemi, Geothermal energy and carbon emissions nexus in leading geothermal-consuming nations: evidence from nonparametric analysis, Energy Environ. (2023) 0958305X231153972, https://doi.org/10.1177/0958305X231153972.

[7] T.M. Letcher, 1 - why do we have global warming? in: T.M. Letcher (Ed.), Manag. Glob. Warm. Academic Press, 2019, pp. 3–15, https://doi.org/10.1016/B978-0-12-814104-5.00001-6.

[8] R. Schmalensee, T.M. Stoker, R.A. Judson, World carbon dioxide emissions: 1950–2050, Rev. Econ. Stat. 80 (1998) 15–27, https://doi.org/10.1162/003465398557294.

[9] V. Ramanathan, Y. Xu, The Copenhagen Accord for limiting global warming: criteria, constraints, and available avenues, Proc Natl Acad Sci 107 (2010) 8055–8062, https://doi.org/10.1073/pnas.1002293107.

[10] J.H. Williams, A. DeBenedictis, R. Ghanadan, A. Mahone, J. Moore, W.R. Morrow, et al., The technology path to deep greenhouse gas emissions cuts by 2050: the pivotal role of electricity, Science 335 (2012) 53–59, https://doi.org/10.1126/science.1208365.

[11] A.J. Weaver, K. Zickfeld, A. Montenegro, M. Eby, Long term climate implications of 2050 emission reduction targets, Geophys. Res. Lett. 34 (2007), https://doi.org/10.1029/2007GL031018.

[12] P. Madejski, K. Chmiel, N. Subramanian, T. Kuś, Methods and techniques for CO2 capture: review of potential solutions and applications in modern energy technologies, Energies 15 (2022) 887, https://doi.org/10.3390/en15030887.

[13] H.A. Alalwan, A.H. Alminshid, CO2 capturing methods: chemical looping combustion (CLC) as a promising technique, Sci. Total Environ. 788 (2021) 147850, https://doi.org/10.1016/j.scitotenv.2021.147850.

[14] O.A. Odunlami, D.A. Vershima, T.E. Oladimeji, S. Nkongho, S.K. Ogunlade, B.S. Fakinle, Advanced techniques for the capturing and separation of CO2 – a review, Results Eng 15 (2022) 100512, https://doi.org/10.1016/j.rineng.2022.100512.

[15] Y. Yu, Y. Du, Impact of technological innovation on CO2 emissions and emissions trend prediction on 'New Normal' economy in China, Atmospheric Pollut Res 10 (2019) 152–161, https://doi.org/10.1016/j.apr.2018.07.005.

[16] L. Lv, Z. Wu, L. Zhang, B.B. Gupta, Z. Tian, An edge-AI based forecasting approach for improving smart microgrid efficiency, IEEE Trans Ind Inform 18 (2022) 7946–7954, https://doi.org/10.1109/TII.2022.3163137.

[17] A. Masood, K. Ahmad, A review on emerging artificial intelligence (AI) techniques for air pollution forecasting: fundamentals, application and performance, J. Clean. Prod. 322 (2021) 129072, https://doi.org/10.1016/j.jclepro.2021.129072.

[18] A. Masood, M. Niazkar, M. Zakwan, R. Piraei, A machine learning-based framework for water quality index estimation in the southern bug river, Water 15 (2023) 3543, https://doi.org/10.3390/w15203543.

[19] R.M. Adnan, R.R. Mostafa, H.-L. Dai, S. Heddam, A. Masood, O. Kisi, Enhancing accuracy of extreme learning machine in predicting river flow using improved reptile search algorithm, Stoch. Environ. Res. Risk Assess. 37 (2023) 3063–3083, https://doi.org/10.1007/s00477-023-02435-y.

[20] A.N. Ahmed, T. Van Lam, N.D. Hung, N. Van Thieu, O. Kisi, A. El-Shafie, A comprehensive comparison of recent developed meta-heuristic algorithms for streamflow time series forecasting problem, Appl. Soft Comput. 105 (2021) 107282, https://doi.org/10.1016/j.asoc.2021.107282.

[21] O. Abedinia, N. Amjady, N. Ghadimi, Solar energy forecasting based on hybrid neural network and improved metaheuristic algorithm, Comput. Intell. 34 (2018) 241–260, https://doi.org/10.1111/coin.12145.

[22] A. Masood, M.M. Hameed, A. Srivastava, Q.B. Pham, K. Ahmad, S.F.M. Razali, et al., Improving PM2.5 prediction in New Delhi using a hybrid extreme learning machine coupled with snake optimization algorithm, Sci. Rep. 13 (2023) 21057, https://doi.org/10.1038/s41598-023-47492-z.

[23] A. Lashgari, H. Hosseinzadeh, M. Khalilzadeh, B. Milani, A. Ahmadisharaf, S. Rashidi, Transportation energy demand forecasting in Taiwan based on metaheuristic algorithms, Energy Sources, Part A Recovery, Util. Environ. Eff. 44 (2022) 2782–2800, https://doi.org/10.1080/15567036.2022.2062072.

[24] B.H. Ismael, F. Khaleel, S.S. Ibrahim, S.R. Khaleel, M.K. AlOmar, A. Masood, et al., Permeation flux prediction of Vacuum Membrane distillation using hybrid machine learning techniques, Membranes 13 (2023) 900, https://doi.org/10.3390/membranes13120900.

[25] X. Qin, S. Zhang, X. Dong, Y. Zhan, R. Wang, D. Xu, China's carbon dioxide emission forecast based on improved marine predator algorithm and multi-kernel support vector regression, Environ. Sci. Pollut. Res. 30 (2023) 5730–5748, https://doi.org/10.1007/s11356-022-22302-7.

[26] S.A. Jalaee, A. Shakibaei, H. Akbarifard, H.R. Horry, A. GhasemiNejad, F. Nazari Robati, et al., A novel hybrid method based on Cuckoo optimization algorithm and artificial neural network to forecast world's carbon dioxide emission, MethodsX 8 (2021) 101310, https://doi.org/10.1016/j.mex.2021.101310.

[27] E. Uzlu, Estimates of greenhouse gas emission in Turkey with grey wolf optimizer algorithm-optimized artificial neural networks, Neural Comput. Appl. 33 (2021) 13567–13585, https://doi.org/10.1007/s00521-021-05980-1.

[28] D.H. Wolpert, W.G. Macready, No free lunch theorems for optimization, IEEE Trans. Evol. Comput. 1 (1997) 67–82, https://doi.org/10.1109/4235.585893.

[29] O.R. Adegboye, E. Deniz Ülker, Hybrid artificial electric field employing cuckoo search algorithm with refraction learning for engineering optimization problems, Sci. Rep. 13 (2023) 4098, https://doi.org/10.1038/s41598-023-31081-1.

[30] O.R. Adegboye, A.K. Feda, O.R. Ojekemi, E.B. Agyekum, B. Khan, S. Kamel, DGS-SCSO: enhancing sand cat swarm optimization with dynamic pinhole imaging and golden sine algorithm for improved numerical optimization performance, Sci. Rep. 14 (2024) 1491, https://doi.org/10.1038/s41598-023-50910-x.

[31] H. Faris, S. Mirjalili, I. Aljarah, M. Mafarja, A.A. Heidari, Salp swarm algorithm: theory, literature review, and application in extreme learning machines, in: S. Mirjalili, J. Song Dong, A. Lewis (Eds.), Nat.-Inspired Optim. Theor. Lit. Rev. Appl., Springer International Publishing, Cham, 2020, pp. 185–199, https://doi.org/10.1007/978-3-030-12127-3_11.

[32] T. Si, P.B.C. Miranda, D. Bhattacharya, Novel enhanced Salp Swarm Algorithms using opposition-based learning schemes for global optimization problems, Expert Syst. Appl. 207 (2022) 117961, https://doi.org/10.1016/j.eswa.2022.117961.

[33] A.K. Mahapatra, N. Panda, B.K. Pattanayak, Quantized salp swarm algorithm (QSSA) for optimal feature selection, Int. J. Inf. Technol. 15 (2023) 725–734, https://doi.org/10.1007/s41870-023-01161-6.

[34] W. Luo, H. Jin, H. Li, X. Fang, R. Zhou, Optimal performance and application for firework algorithm using a novel chaotic approach, IEEE Access 8 (2020) 120798–120817, https://doi.org/10.1109/ACCESS.2020.3004430.

[35] M. Zhang, D. Wang, J. Yang, Hybrid-flash butterfly optimization algorithm with logistic mapping for solving the engineering constrained optimization problems, Entropy 24 (2022) 525, https://doi.org/10.3390/e24040525.

[36] C. Li, J. Li, H. Chen, A meta-heuristic-based approach for qos-aware service composition, IEEE Access 8 (2020) 69579–69592, https://doi.org/10.1109/ACCESS.2020.2987078.

[37] H.R. Tizhoosh, Opposition-based learning: a new scheme for machine intelligence, in: Int. Conf. Comput. Intell. Model. Control Autom. Int. Conf. Intell. Agents Web Technol. Internet Commer, CIMCA-IAWTIC06, 2005, pp. 695–701, https://doi.org/10.1109/CIMCA.2005.1631345, vol. 1.

[38] L. Yao, P. Yuan, C.-Y. Tsai, T. Zhang, Y. Lu, S. Ding, ESO: an enhanced snake optimizer for real-world engineering problems, Expert Syst. Appl. 230 (2023) 120594, https://doi.org/10.1016/j.eswa.2023.120594.

[39] X.-S. Yang, S. Deb, Engineering optimisation by cuckoo search. https://doi.org/10.48550/arXiv.1005.2908, 2010.

[40] S. Mirjalili, S.M. Mirjalili, A. Lewis, Grey wolf optimizer, Adv Eng Softw 69 (2014) 46–61, https://doi.org/10.1016/j.advengsoft.2013.12.007.

[41] S. Mirjalili, A.H. Gandomi, S.Z. Mirjalili, S. Saremi, H. Faris, S.M. Mirjalili, Salp Swarm Algorithm: a bio-inspired optimizer for engineering design problems, Adv Eng Softw 114 (2017) 163–191, https://doi.org/10.1016/j.advengsoft.2017.07.002.

[42] C. Cortes, V. Vapnik, Support-vector networks, Mach. Learn. 20 (1995) 273–297, https://doi.org/10.1007/BF00994018.

[43] O. Adegboye, M. Aldağ, E.D. Ülker, Support vector machines in determining the characteristic impedance of microstrip lines, in: J. Hemanth, T. Yigit, B. Patrut, A. Angelopoulou (Eds.), Trends Data Eng. Methods Intell. Syst., Springer International Publishing, Cham, 2021, pp. 400–408, https://doi.org/10.1007/978-3-030-79357-9_39.

[44] J. Li, B. Zhang, J. Shi, Combining a genetic algorithm and support vector machine to study the factors influencing CO2 emissions in Beijing with scenario analysis, Energies 10 (2017) 1520, https://doi.org/10.3390/en10101520.

[45] A. Malik, Y. Tikhamarine, D. Souag-Gamane, O. Kisi, Q.B. Pham, Support vector regression optimized by meta-heuristic algorithms for daily streamflow prediction, Stoch. Environ. Res. Risk Assess. 34 (2020) 1755–1773, https://doi.org/10.1007/s00477-020-01874-1.

[46] H. Zhong, J. Wang, H. Jia, Y. Mu, S. Lv, Vector field-based support vector regression for building energy consumption prediction, Appl. Energy 242 (2019) 403–414, https://doi.org/10.1016/j.apenergy.2019.03.078.

[47] I. Karakurt, G. Aydin, Development of regression models to forecast the CO2 emissions from fossil fuels in the BRICS and MINT countries, Energy 263 (2023) 125650, https://doi.org/10.1016/j.energy.2022.125650.

[48] K.R. Abbasi, M. Shahbaz, J. Zhang, M. Irfan, R. Alvarado, Analyze the environmental sustainability factors of China: the role of fossil fuel energy and renewable energy, Renew. Energy 187 (2022) 390–402, https://doi.org/10.1016/j.renene.2022.01.066.
[49] A. Bibi, X. Zhang, M. Umar, The imperativeness of biomass energy consumption to the environmental sustainability of the United States revisited, Environ. Ecol. Stat. 28 (2021) 821–841, https://doi.org/10.1007/s10651-021-00500-9.
[50] J. Gao, L. Zhang, Does biomass energy consumption mitigate CO2 emissions? The role of economic growth and urbanization: evidence from developing Asia, J. Asia Pac. Econ. 26 (2021) 96–115, https://doi.org/10.1080/13547860.2020.1717902.